An eigenvalue-based similarity measure and its application in defect detection

by

Du-Ming Tsai, Ron-Hwa Yang

Department of Industrial Engineering and Management
Yuan-Ze University, Taiwan, R.O.C.

Corresponding author:

Du-Ming Tsai
Department of Industrial Engineering & Management
Yuan-Ze University
135 Yuan-Tung Road
Nei-Li, Tao-Yuan
Taiwan, R.O.C.

Tel: (03) 463-8800
Fax: (03) 463-8907
E-mail: iedmtsai@saturn.yzu.edu.tw

An eigenvalue-based similarity measure and its application in defect detection

ABSTRACT

In this paper, we propose an eigenvalue-based similarity measure between two gray-level images and, in particular, aim at the application in defect detection. The pair-wise gray levels at coincident pixel locations in two compared images are used as the coordinates to plot the correspondence map. If two compared images are identical, the plot in the correspondence map is a diagonal straight line. Otherwise, it results in a non-linear shape in the correspondence map. The smaller eigenvalue of the covariance matrix of the data points in the correspondence map is used as the similarity measure. It will be approximately zero for two resembled images, and distinctly large for dissimilar images. Experimental results from a number of assembled PCBs (printed circuit boards) have shown the effectiveness of the proposed similarity measure for detecting local defects in complicated images.

Keywords: Similarity measure; Defect detection; Eigenvalues; Template matching

1. INTRODUCTION

Normalized cross correlation has long been a common and powerful similarity measure in computer vision, which has been extensively used for applications such as object recognition [1, 2], OCR [3, 4] and defect inspection [5-8].

The traditional normalized cross correlation between a scene image f and a reference template w is given by [9]:

$$\gamma = \frac{\sum_{x=0}^{m-1}\sum_{y=0}^{n-1}\left[f(x,y)-\overline{f}\right]\cdot\left[w(x,y)-\overline{w}\right]}{\left\{\sum_{x=0}^{m-1}\sum_{y=0}^{n-1}\left[f(x,y)-\overline{f}\right]^2\cdot\sum_{x=0}^{m-1}\sum_{y=0}^{n-1}\left[w(x,y)-\overline{w}\right]^2\right\}^{1/2}} \tag{1}$$

where $m\times n$ is the size of the neighborhood window; $\overline{f}$ and $\overline{w}$ are the mean gray values of the windowed subimages in f and w, respectively. The normalized correlation γ is scaled in the range -1 to 1, and a prefect match between f and w will have a maximum value of unity. In object recognition applications, one finds a desired pattern in the scene image by sliding the window of a reference template in a pixel-by-pixel basis, and computing the correlation between the two windowed subimages. The peak of the correlation value indicates an instance of the template in the scene image.

In defect inspection applications, the normalized cross correlation between two windowed subimages at coincident locations in their respective scene image and faultless reference image is calculated, and the process is repeated for all pixels in the

whole image. A pixel with small γ value below some predetermined threshold is classified as a defective point. When the normalized cross correlation is applied as a similarity (or dissimilarity) measure for defect detection, it may not be sufficiently responsive to the detection of subtle anomalies, and may result in false acceptance. Figure 1(a) shows the reference image of a partial printed circuit board (PCB), and Figure 1(b) is a faultless image of the PCB. The dotted squares of size 30×30 pixels in Figures 1(a)-(c) mark the test subimages for comparison. The resulting γ value between Figures 1(a) and 1(b) is 0.99, which indicates that the two compared images are nearly identical. Figure 1(c) is a defective version of the PCB, where the printed digit "2" is blurred. The correlation value of the two compared subimages in Figures 1(a) and 1(c) is as high as 0.86, and the image under inspection might be falsely accepted as a faultless one.

Image difference operations that subtract the scene image from the template image are simple and efficient for defect detection applications in industry. Wu et al. [10] directly subtracted the inspection image from the template image in binary mode for PCB defect detection. They then applied an elimination process to distinguish true defects from noise in the residual image. Ibrahim et al. [11] and Ibrahim and Al-Attas [12] also applied the image difference operation for PCB inspection. Instead of doing the subtraction in the binary images, the difference operation is carried out in the wavelet-domain image in order to minimize computation time. Yazdi and King [13] developed an automatic vision system for inspection of lace fabric in binary mode. They first used a correlation measure to align the inspection image so that it has the same size and orientation as the template image. Direct subtraction is then applied to the aligned image and the template image.

Morphological filtering is finally used to remove residues in the difference image. The existing image difference algorithms are very efficient and effective for detecting defects in binary images. They are prone to failure for complicated gray-level images due to illumination changes.

Our work has been motivated by a need to develop an effective similarity measure that can be significantly responsive to local deviations between two compared images. In this study, we propose an eigenvalue-based similarity measure between two gray-level images and, in particular, focus on the application in defect inspection. The proposed similarity measure is based on the shape of the pair-wise gray-level distribution of two compared images. Given a reference image $w(x, y)$ and a scene image $f(x, y)$, we may plot the gray-level distribution of the two images in a 2D map with coordinates $[w(x, y), f(x, y)]$ for each image pixel (x, y). The resulting 2D gray-level distribution is named gray-level correspondence map, in which the gray-level distribution will be a diagonal line if images f and w are perfectly identical, and the distribution will be a nonlinear shape if the two compared images are different. The shape of gray-level distribution is then measured by the eigenvalues of the covariance matrix of the data points in the 2D gray-level correspondence map. The smaller eigenvalue of the covariance matrix is used as the similarity measure of two compared images. It will be approximately zero if the two compared images are identical, whereas it will be distinctly large if the two compared images are different to some extent. The discrimination capabilities of the proposed similarity measure, the traditional normalized cross correlation, and the image difference operation are also evaluated in the study.

This paper is organized as follows: Section 2 first describes the representation of the 2D gray-level correspondence map, and discusses the shapes of gray-level distributions of various image contents in the correspondence maps. Then the eigenvalue of the covariance matrix used for describing the shape of gray-level distribution in the correspondence map is presented. Section 3 discusses the experimental results from a number of assembled PCBs. Effects of changes in window size and illumination are also analyzed. The paper is concluded in Section 4.

2. PAIR-WISE GRAY-LEVEL CORRESPONDENCE MAP

Let $f(x, y)$ and $w(x, y)$ be the gray levels of the respective scene image and reference image at pixel coordinates (x, y), and $f(x, y), w(x, y) \in \{0,1,2,..., L\}$. The pair-wise gray values at coincident pixel locations in the two compared images are used as the coordinates to plot the correspondence map, where the *x*-axis is the gray level for the reference image w, and the *y*-axis is the gray level for the scene image f. The scales of each axis in the correspondence map are $0, 1, 2,..., L$. For each pixel coordinates (x, y) in the image, a correspondence point with coordinates $[w(x, y), f(x, y)]$ is generated in the 2D gray-level correspondence map. Since different pixel coordinates in the image may result in the same correspondence point in the 2D map, the transformation is a many-to-one correspondence. Let $m \times n$ be the neighborhood window size, and $C[i, j]$ the accumulated number of pixels that has gray value *i* in the reference image w, and the corresponding gray value *j* in the scene image f. That is

For $x = 0, 1, 2, \ldots, m\text{-}1$

For $y = 0, 1, 2, \ldots, n\text{-}1$

$$C[w(x,y), f(x,y)] = C[w(x,y), f(x,y)] + 1$$

Next y

Next x

If f and w are two identical gray-level images, then the correspondence map $C[i, j]$ will be a diagonal straight line. Depending on the degree of difference between f and w, the gray-level distribution in the correspondence map will deviate from the diagonal line, and form a shape of non-linear structure.

In order to visualize the gray-level distribution in the correspondence map, $C[i, j]$ is represented as an intensity function, where darkness is proportional to the magnitude of $C[i, j]$. Figures 2(a) and 2(b1) show a reference image (a partial IC mark), and a test image under the same lighting conditions. Figures 2(b2) and 2(b3) are the overexposed and underexposed versions of the test sample. Figures 2(c1)-(c3) are the resulting gray-level correspondence maps for the test images in Figures 2(b1)-(b3), respectively. It can be seen from Figure 2 that the plot in the correspondence map is approximately a straight line and varies according to the lighting condition. A fine 45° straight line is generated for the two identical images (Figures 2(a) vs. 2(b1)). A bold straight line (due to non-uniform illumination) with slop angle larger than 45° is obtained for the overexposed image in Figure 2(b2). In contrast, a line with slop angle less than 45° is obtained for the underexposed image in Figure 2(b3). Therefore, if two compared images have the same contents, a straight line will be generated in the 2D gray-level correspondence

map, and the slop angle of the line represents the variation of illumination between the scene and reference images.

Figure 3(a) shows the reference image of a partial IC mark, and Figure 3(b) is a defective version of the IC mark under the same lighting conditions. Figure 3(c) is the gray-level correspondence map of Figure 3(a) vs. 3(b). It can be seen from Figure 3(c) that a diagonal straight line is generated in the correspondence map, which represents the identical regions of the two compared images. The points deviated from the diagonal line in the correspondence map correspond to the defective region in the scene image. Figure 3(e) shows the resulting 2D gray-level correspondence map from Figures 3(a) and (d). These two compared images have completely different contents. No diagonal straight line can be observed in the correspondence map of these two heterogeneous images.

Figure 4 presents the result of two approximately uniform images. A small spot along the diagonal direction is obtained in the resulting gray-level correspondence map. Figure 5 shows the result of two resembled test images that contain only a few high-contrast gray levels. The resulting correspondence map shows a few spots distributed along the diagonal direction, which correspond to the discrete high-contrast gray values in the original images.

3. THE SIMILARITY MEASURE

In this paper, the measure of the shape (and thus, the similarity between two

compared images) in the correspondence map is derived from the statistical and geometric properties associated with the eigenvalues of the covariance matrix of the data points in the correspondence map.

The covariance matrix M of a reference image $w(x,y)$ and a scene subimage $f(x,y)$, both of size $m \times n$, in the gray-level correspondence map is given by

$$M = \begin{bmatrix} m_{11} & m_{12} \\ m_{21} & m_{22} \end{bmatrix} \tag{2}$$

where $$m_{11} = \left[\frac{1}{m \times n} \sum_{x=0}^{m-1} \sum_{y=0}^{n-1} f^2(x,y) \right] - (\overline{f})^2$$

$$m_{22} = \left[\frac{1}{m \times n} \sum_{x=0}^{m-1} \sum_{y=0}^{n-1} w^2(x,y) \right] - (\overline{w})^2$$

$$m_{12} = m_{21} = \left[\frac{1}{m \times n} \sum_{x=0}^{m-1} \sum_{y=0}^{n-1} f(x,y) \cdot w(x,y) \right] - (\overline{f} \cdot \overline{w})$$

$\overline{f}$ and $\overline{w}$ are the mean gray values of $f(x,y)$ and $w(x,y)$, respectively, i.e.,

$$\overline{f} = \frac{1}{m \times n} \sum_{x=0}^{m-1} \sum_{y=0}^{n-1} f(x,y)$$

$$\overline{w} = \frac{1}{m \times n} \sum_{x=0}^{m-1} \sum_{y=0}^{n-1} w(x,y)$$

Note that the covariance matrix M can be directly calculated from gray-level images $f(x,y)$ and $w(x,y)$. The 2D gray-level correspondence map is only

conceptually constructed. The covariance matrix is 2×2, symmetric and positive semidefinite. There are two eigenvalues λ_L and λ_S for the matrix M, which are [14]

$$\lambda_L = \frac{1}{2}\left[m_{11} + m_{22} + \sqrt{(m_{11} - m_{22})^2 + 4m_{12}^2}\right] \tag{3}$$

$$\lambda_S = \frac{1}{2}\left[m_{11} + m_{22} - \sqrt{(m_{11} - m_{22})^2 + 4m_{12}^2}\right] \tag{4}$$

$$\lambda_S \le \lambda_L$$

The eigenvalues of the matrix M can be used to extract the shape information about the gray-level distribution in the correspondence map. The larger eigenvalue λ_L represents the variance of data along the major-axis of the shape, and the smaller eigenvalue λ_S represents the variance of data along the minor-axis of the shape in the 2D correspondence map. If the shape is a straight line, i.e., two compared images are identical, in the gray-level correspondence map, the smaller eigenvalue λ_S will have an ideal value of zero since the variance along the minor-axis of a line is zero. The eigenvalue λ_S will be distinctly large if the shape formed in the gray-level correspondence map is not a straight line. Therefore, the smaller eigenvalue λ_S of the covariance matrix M is adopted as a similarity measure between two compared images.

Note that the traditional normalized cross correlation, as formulated in eq. (1), can also be expressed with m_{11}, m_{22} and m_{12}, i.e.,

$$\gamma = \frac{m_{12}}{\sqrt{m_{11} \cdot m_{22}}} \tag{5}$$

As aforementioned, the correlation value between the two compared subimages of size 30×30 pixels in Figures 1(a) and 1(c) is as high as 0.86. The respective λ_S values from the faultless image (Figure 1(b)) and the defect image (Figure 1(c)) are 0.15 and 528.94. They are distinctly different in magnitude. The results reveal that the similarity measure λ_S is superior to the normalized cross correlation γ for detecting small anomalies in a complicated gray-level image.

The comparison between the resulting correlation value γ and eigenvalue λ_S from the test images in Figures 2-5 is summarized in Table 1. Note that the resulting measures in Table 1 are derived from the subimages of size 100×100 pixels in Figures 2-5. It is apparent from the table that the eigenvalue λ_S is an effective measure to discriminate the difference between two compared images. The resulting λ_S values are quite small for resembled images, but distinctly large for dissimilar images.

When a uniform image is compared with any arbitrary reference image, the resulting eigenvalue λ_S is also approximately zero. Since the linear distribution of two such images will be vertical or horizontal in the correspondence map, the orientation of the line is far away from the 45°-diagonal direction. The line orientation in the correspondence map can be easily determined from the eigenvector associated with the major axis. The eignevalue λ_S along with the line orientation can sufficiently identify anomalies in two compared images. Since both the similarity measure λ_S an the normalized cross correlation γ can be computed from m_{11}, m_{22} and m_{12} in eq. (2), we may alternately use λ_S as the supplement of γ for defect detection, i.e., a defect is reported whenever the corresponding γ value is

sufficiently small or the λ_S value is sufficiently large.

The inherited limitation to both the proposed similarity measure λ_S and the normalized cross-correlation γ is their sensitivity to image translation. To overcome the effect of shifting, one may have to search for the local minimum value of λ_S in a small search region, i.e.,

$$\lambda_S(x, y) = \min_{(i,j)}\{\lambda_S(x+i, y+j)\}$$

where $\lambda_S(x+i, y+j)$ is the eigenvalue λ_S at coordinates $(x+i, y+j)$, and (i, j) defines the search region of a tolerable image translation. Note that the search needs only to be carried out for those candidates of defective pixels that have significantly large λ_S values.

4. EXPERIMENTAL RESULTS

In this section, we present the experimental results for evaluating the efficacy of the proposed similarity measure. The images are 400×400 pixels wide with 8-bit gray levels. In the experiments, we especially focus on the use of similarity measures for defect inspection applications. In order to visualize the detection results of two compared images, the resulting values of λ_S (or $1-\gamma$) are represented as an intensity function, where darkness is proportional to the magnitude of λ_S (or $1-\gamma$). A large value of λ_S (or $1-\gamma$) will result in a dark intensity region in the resulting image. The darker the intensity in the resulting image, the stronger the evidence of a defect. The effects of changes in window size and

illumination are first discussed.

Test samples in Figure 6 are used to evaluate the effect of varying window sizes on the detection results of the similarity measure λ_S. Figure 6(a) shows the image of a faultless assembled PCB used as a reference. Figures 6(b) and (c) are respectively a defect-free version and a defect image of the PCB. In the experiment, the window size is varied from 5×5, 20×20 to 35×35. Figures 6(d)-(f) show the detection results of the defect-free PCB (Figure 6(b)) from window sizes 5×5, 20×20 and 35×35 pixels, respectively. The detection results of the defective PCB (Figure 6(c)) are presented in Figures 6(g)-(i). The detection results show that the small window size of 5×5 contains little structure of the image content and, therefore, generates much noise in the defect-free image. The detected defect area in the defective PCB image with the small window size is less visible and distributes in a scattering manner. A large window size of 35×35 may not generate better detection, and increases the computation burden. In terms of detection effectiveness and computational efficiency, the suggested window width for defect detection is in the range between 20 and 30 pixels.

In order to evaluate the effect of changes in illumination, Figure 7(a) shows a reference PCB image at illumination 340 Lux, and Figures 7(b)-(f) are defective versions of the PCB at 340, 440, 500, 240 and 200 Luxes, respectively. The neighborhood window used for the test is 20×20 pixels. The resulting similarity measures of $1-\gamma$ and λ_S as an intensity function are presented in Figures 8(a1)-(a5) and 8(b1)-(b5). They show that the defective region is well detected using the similarity measure λ_S for the test sample under varying illumination levels.

The normalized cross correlation can also detect faults, but with more noisy points in the resulting images. The results also reveal that both λ_S and γ measures are less sensitive to overexposed images, whereas their performance is degraded for severely underexposed images. This is because that an overexposed image preserves a better linearity of illumination changes in the correspondence map, compared to that of a highly underexposed image.

To further compare the performance between the proposed similarity measure λ_S and the commonly used image difference operation, Figures 8(c1)-(c5) show respectively the subtraction results of the inspection images at illumination levels 500, 400, 340, 240 and 200 Lux from the reference image at illumination 340 Lux, in which darkness is linearly proportional to the magnitude of the subtracted values. It can be observed from Figure 8(c3) that the defective region can be well detected if the inspection image and the reference image are at the same illumination level. Many light residual pixels appear as noise in the difference image of Figure 8(c3). As the inspection images with illumination levels apart from 340 Lux, the residual pixels become darker and increase in number. They may cause serious false alarms. Conversely, the proposed similarity measure λ_S makes the normal region consistently white in the resulting image, regardless of the changes in illumination level from 240 to 500 Lux.

In order to further demonstrate the effectiveness of the proposed similarity measure λ_S, defect detection of SMT (surface-mounted technology) components on PCBs is examined in the experiment. Figure 9(b) shows a displaced (rotated by a small angle) SMT component. Figure 10(b) shows an SMT component with wrong

polarity (the component is mounted in a 180^{o} reverse on the PCB and, therefore, the printed characters on the component are reversed). The neighborhood window used for these test samples is 30×30 pixels. The detection results of the two SMT samples from the similarity measures of $1-\gamma$ and λ_S are presented in Figures 9(c)-(d) and Figures 10(c)-(d), respectively. As seen in Figures 9 and 10, the proposed similarity measure λ_S can reliably detect the defective regions, even though the SMT components show only minor variations from their faultless references. Since the proposed similarity measure λ_S can be well responsive to local deviations, it is especially suited for the detection of mis-registered SMT components on PCBs.

4. CONCLUSIONS

In defect detection applications, the traditional normalized cross correlation is a good indicator to detect major difference between two compared images. However, its performance degrades when the two compared images contain only minor difference. In this paper, we have proposed an eigenvalue-based similarity measure between the reference image and the scene image. The core concept of the proposed method is to transform the gray levels of two compared images at each coincident pixel location to form a gray-level pair. Gray-level pairs give the point coordinates to form the 2D gray-level correspondence map. The shape of gray-level pairs distributed in the correspondence map represents the similarity between two compared images. Two identical images result in a fine diagonal straight line, and any two dissimilar images generate non-linear shape of gray-level distribution in the

correspondence map. The smaller eigenvalue λ_S of the covariance matrix of gray-level pairs is used as the similarity measure. The ideal λ_S value will be zero for two identical images, and will be distinctly large for two dissimilar images.

Experimental results have shown that the discrimination capability of the proposed similarity measure is superior to the traditional normalized cross correlation. It is also highly responsive to subtle defects and greatly tolerable to illumination changes, compared to the image difference operation. The proposed method is especially well suited for the application in defect detection. Defects embedded in complicated material surfaces such as printed-circuit boards, surface-mounted devices and IC wafers can be effectively detected using the proposed similarity measure λ_S.

REFERENCES

1. J. Ooi, K. Rao, New insights into correlation-based template matching, Proceedings of SPIE, V. 1468, Applications of Artificial Intelligence IX, Orlando, FL, 1991, pp. 740-751.

2. D.-M. Tsai, C.-H Chiang, Rotation-invariant pattern matching using wavelet decomposition, Pattern Recognition Letters 23 (2002) 191-201.

3. C. Chatterjee, V. Roychowdhury, New training rule for optical recognition of binary character images by spatial correlation, Proceedings of IEEE International Conference on Neural Networks, Part 6, Orlando, FL, 1994, pp. 4095-4100.

4. H. Penz, I. Bajla, A. Vrabl, W. Krattenthaler, K. Mayer, Fast real-time recognition and quality inspection of printed characters via point-correlation, Proceedings of SPIE, V. 4303, Real-Time Imaging V, San Jose, CA, 2001, pp. 127-137.

5. H. H. Szu, Automatic fault recognition by image correlation neural network techniques, IEEE Trans. Industrial Electronics 40 (1993) 197-208.

6. J. H. Kim, H. S. Cho, S. Kim, Pattern classification of solder joint images using a correlation neural network, Engineering Applications of Artificial Intelligence 9 (1996) 655-669.

7. C. E. Costa, M. Petrou, Automatic registration of ceramic titles for the purpose of fault detection, Machine Vision and Applications 11 (2000) 225-230.

8. M.-C. Chang, C.-S, Fuh, H-Y. Chen, Fast search algorithms for industrial inspection, International Journal of Pattern Recognition and Artificial Intell. 15 (2001) 675-690.

9. R. C. Gonzalez, R. E. Woods, Digital Image Processing, Prentice-Hall, Upper Saddle River, NJ, 2002.

10. W. Y. Wu, M. J. Wang, C. M. Liu, Automated inspection of printed circuit boards through machine vision, Computers in Industry 28 (1996) 103-111.

11. Z. Ibrahim, S. A. R. Al-Attas, Z. Aspar, Analysis of the wavelet-based image difference algorithm for PCB inspection, Proceedings of the 41th SICE Annual Conference, Osaka, 2002, pp. 2108-2113.

12. Z. Ibrahim, S. A. R. Al-Attas, Wavelet-based printed circuit board inspection algorithm, Integrated Computer-Aided Engineering 12 (2005) 201-213.

13. H. R. Yazdi, T. G. King, Applications of 'vision in the loop' for inspection of lace fabric, Real-Time Imaging 4 (1998) 317-332.

14. G. Strang, Linear Algebra and Its Applications, Harcourt Brace Jovanovich, Orlando, Florida, 1988.

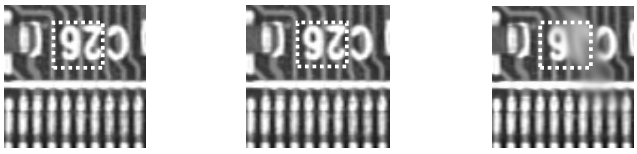

(a) (b) (c)

Figure 1. Images of a partial printed circuit board:
(a) reference image; (b) faultless test image;
(c) defective test image. The dotted squares of size
30×30 pixels mark the subimages for comparison.

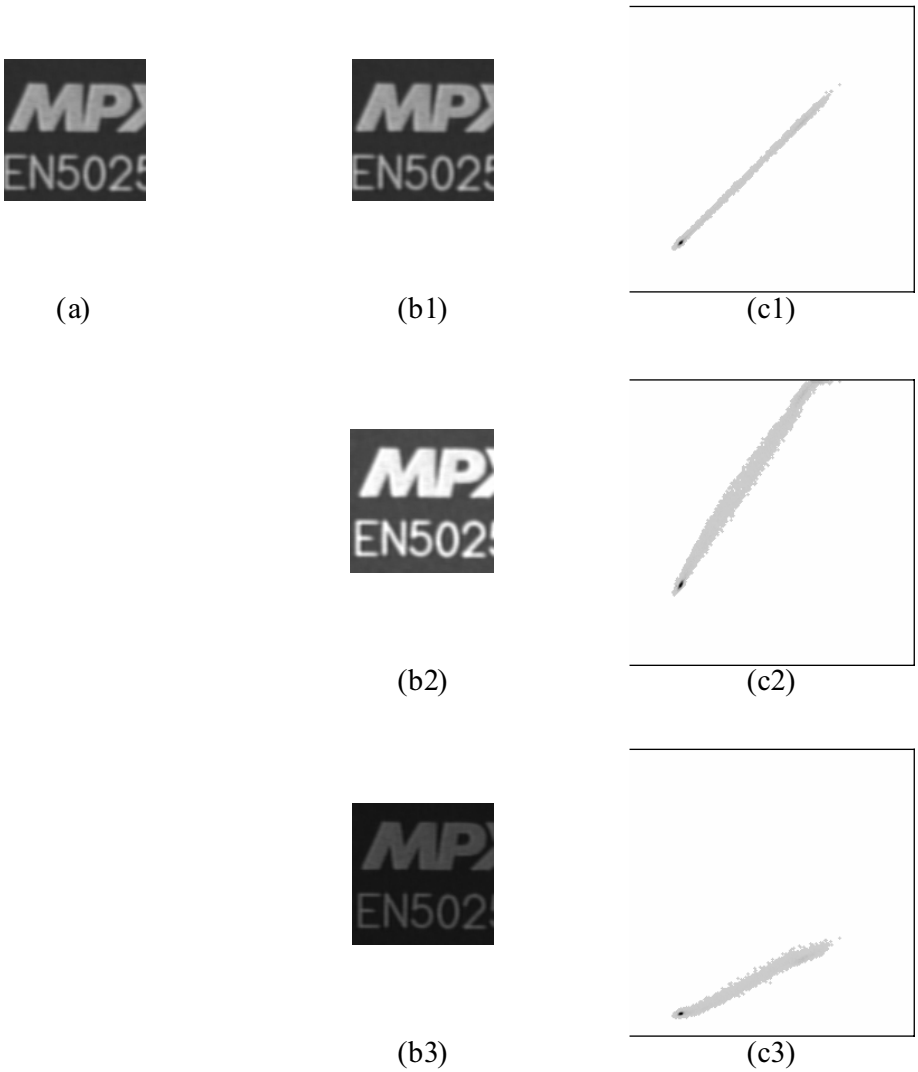

Figure 2. The correspondence maps for two images with the same contents in varying illumination: (a) the reference image of printed characters on an IC; (b1) a faultless test image under the same lighting condition as (a); (b2) an overexposed image; (b3) an underexposed image; (c1)-(c3) the resulting gray-level correspondence maps from (a) vs. (b1), (a) vs. (b2) and (a) vs. (b3), respectively.

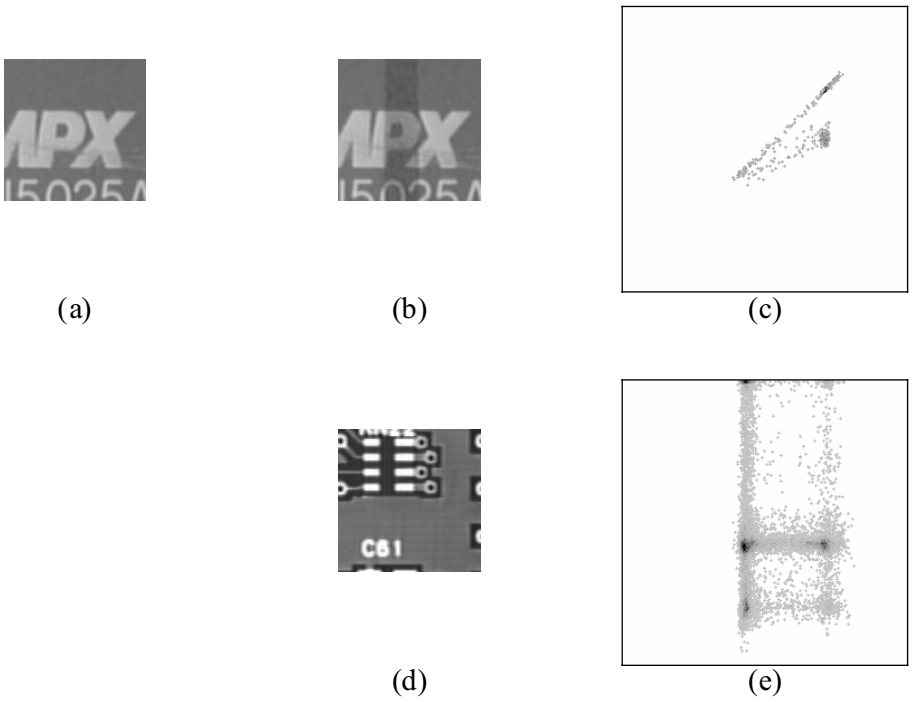

Figure 3. (a) Reference image of IC mark; (b) a defective version of (a); (c) correspondence map of the two images ((a) vs. (b)) with minor difference; (d) a PCB image completely different from (a); (e) correspondence map of the two heterogeneous images ((a) vs. (d)).

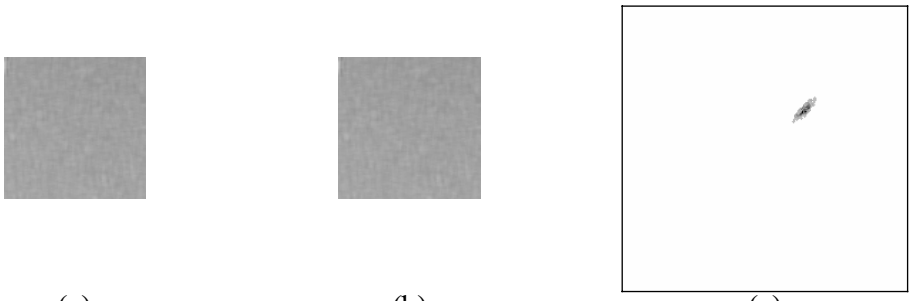

(a) (b) (c)

Figure 4. The correspondence map for two uniform images: (a) the reference image; (b) the scene image; (c) the resulting gray-level correspondence map.

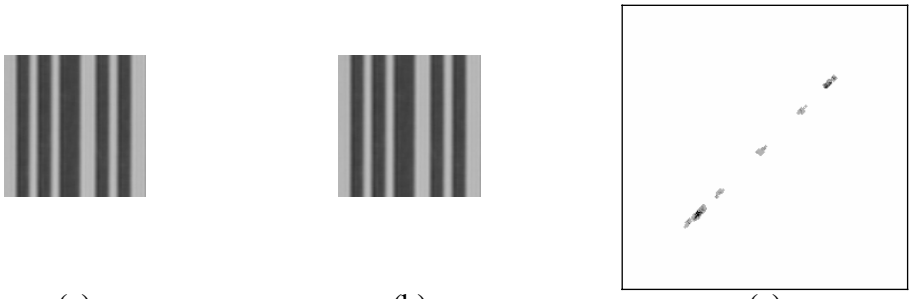

(a) (b) (c)

Figure 5. The correspondence map for two images containing discrete high-contrast gray values: (a) the reference image; (b) the scene image; (c) the resulting gray-level correspondence map.

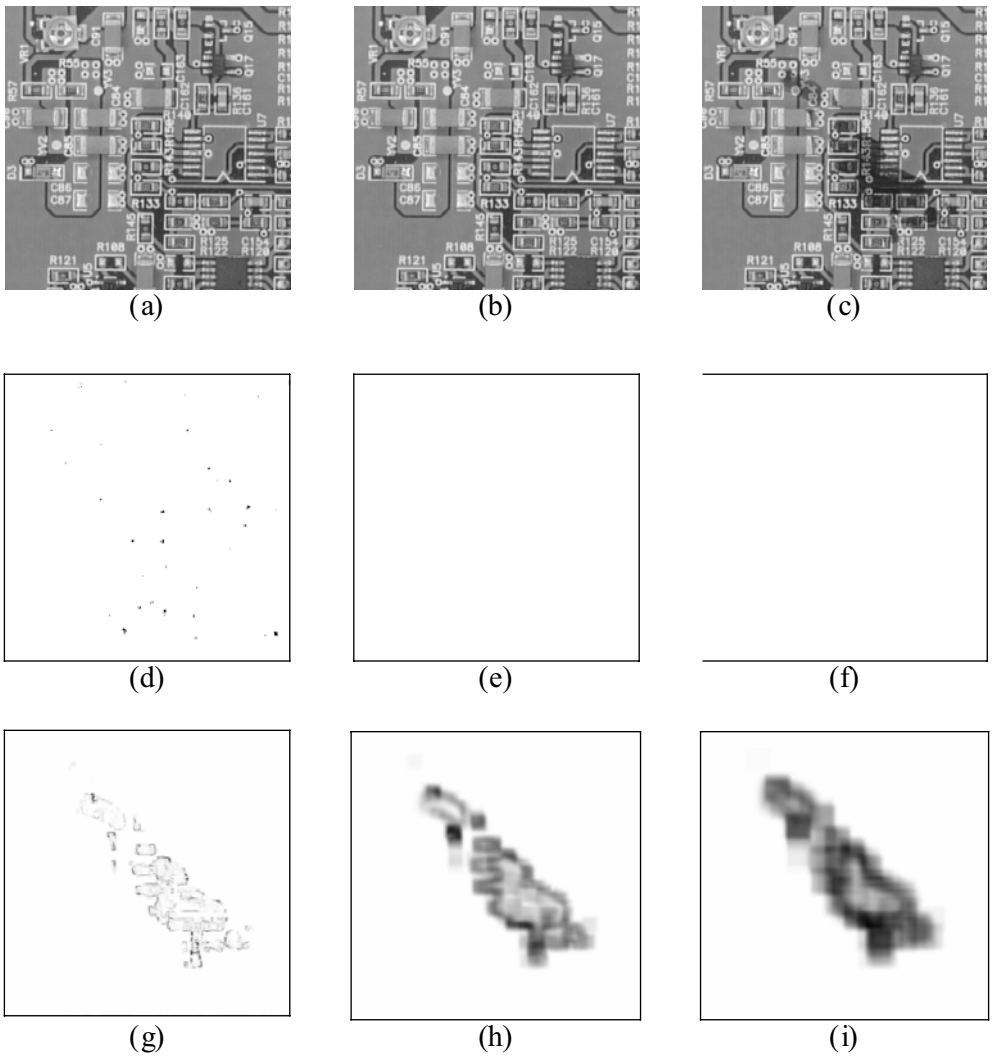

Figure 6. Effect of changes in window size: (a) reference PCB image; (b) faultless PCB image; (c) defective PCB image; (d)-(f) detection results of (a) vs. (b) from window sizes 5×5, 20×20 and 35×35, respectively; (g)-(i) detection results of (a) vs. (c) from respective window sizes.

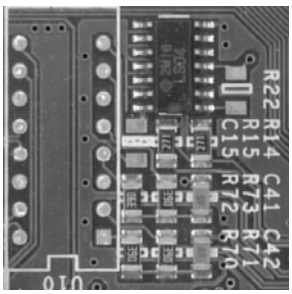
(a) 340Lux

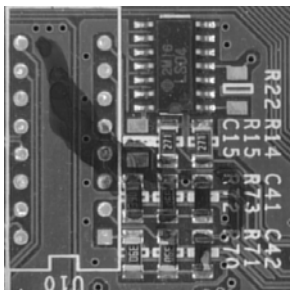
(b) 340Lux

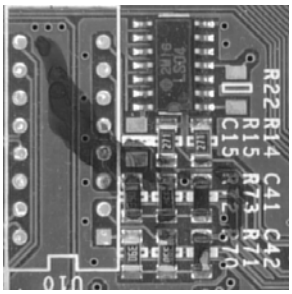
(c) 440Lux

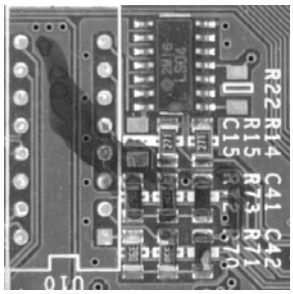
(d) 500Lux

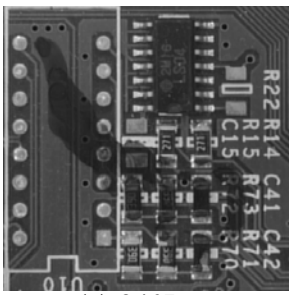
(e) 240Lux

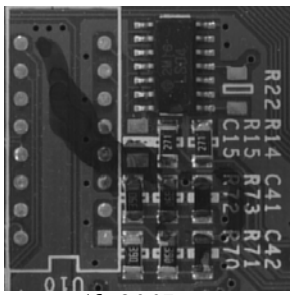
(f) 200Lux

Figure 7. Sample images used to evaluate the effect of changes in illumination: (a) the reference image at 340 Lux; (b)-(f) the scene images at 340,440,500,240 and 200 Luxes, respectively.

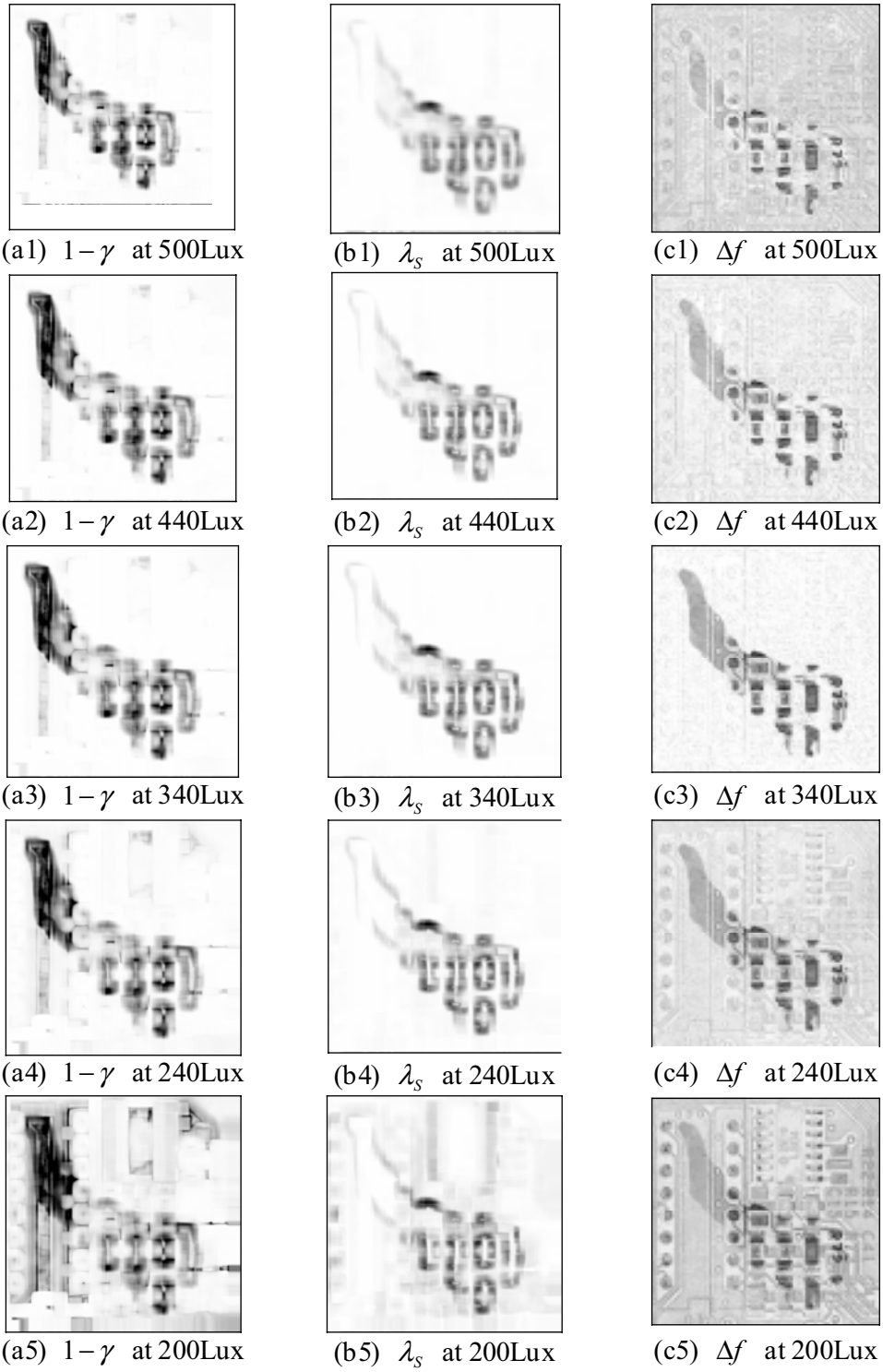

Figure 8. The resulting similarity measures as an intensity function: (a1)-(a5) magnitudes of $1-\gamma$ from images at illumination levels 500, 440, 340, 240 and 200 Luxes; (b1)-(b5) magnitudes of λ_S from images at respective illumination levels; (c1)-(c5) difference images (denoted by Δf) at respective illumination levels.

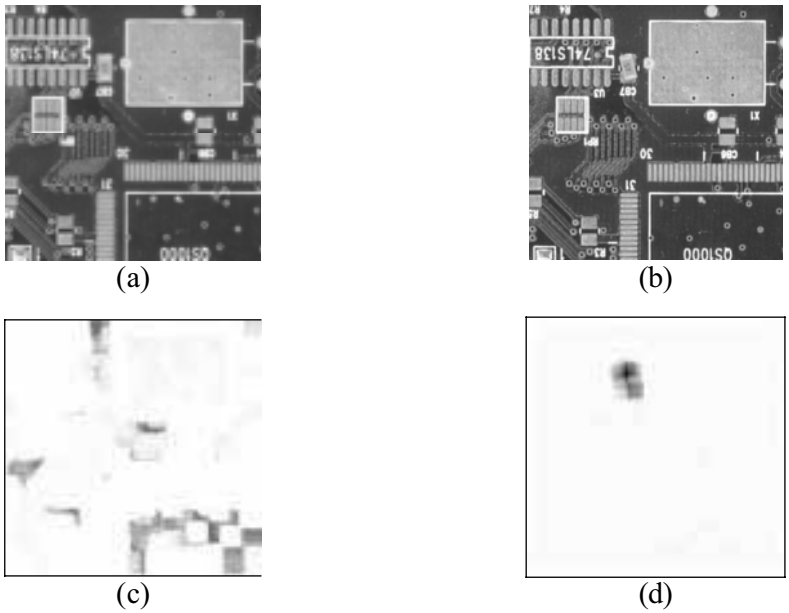

Figure 9. A displaced SMT component on the PCB: (a) the reference image; (b) the defective image; (c), (d) the respective detection results of $1-\gamma$ and λ_S as an intensity function.

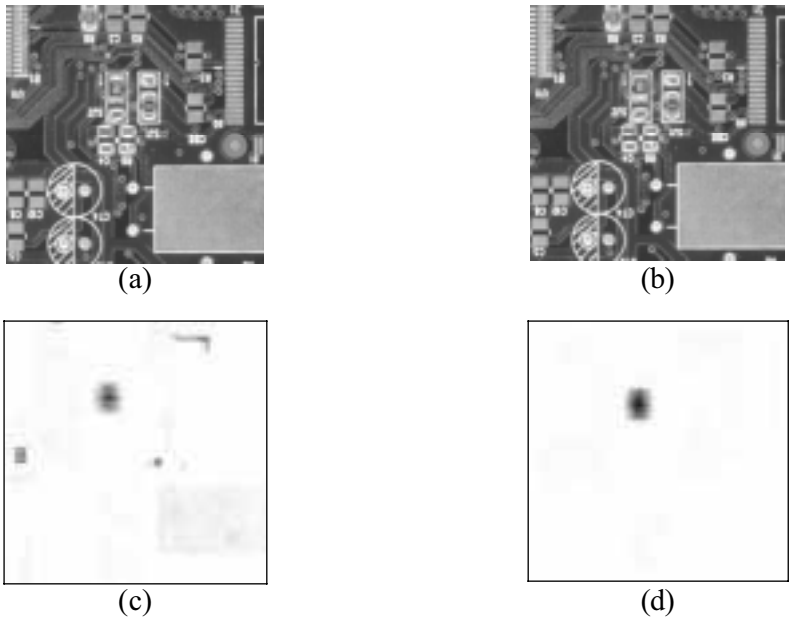

Figure 10. A SMT component with wrong polarity on the PCB: (a) the reference image; (b) the defective image; (c), (d) the respective detection results of $1-\gamma$ and λ_S as an intensity function.

Table 1. The resulting statistics of eigenvalue λ_S and correlation coefficient γ from the test images in Figures 2-5.

Compared images	Similarity measures	
	λ_S	γ
Fig. 2(a) vs. 2(b1)	0.85	0.999
Fig. 2(a) vs. 2(b2)	6.55	0.997
Fig. 2(a) vs. 2(b3)	4.38	0.993
Fig. 3(a) vs. 3(b)	85.08	0.908
Fig. 3(a) vs. 3(d)	949.59	0.000
Fig. 4(a) vs. 4(b)	1.82	0.874
Fig. 5(a) vs. 5(b)	0.81	0.999